Entry of a sphere into a water-surfactant mixture and the effect of a bubble layer

N. B. Speirs, M. M. Mansoor, R. C. Hurd, S. I. Sharker, W. G. Robinson, B. J. Williams, and T. T. Truscott*

Department of Mechanical and Aerospace Engineering, Utah State University, Logan, Utah 84322-4130, USA

(Received 7 July 2017; published 29 October 2018)

A rigid sphere entering a liquid bath does not always produce an entrained air cavity. Previous experimental work shows that cavity formation, or the lack thereof, is governed by fluid properties, wetting properties of the sphere, and impact velocity. In this study, wetting steel spheres are dropped into a water-surfactant mixture with and without passing through a bubble layer first. Surprisingly, in the case of a water-surfactant mixture without a bubble layer, the critical velocity for cavity formation becomes radius dependent. This occurs due to dynamic surface tension effects, with the local surface tension in the splash increasing during surface expansion and decreasing as surfactant molecules adsorb to the newly formed interface. The larger sphere radii take longer to submerge and hence allow more time for the surface tension to decrease back to the equilibrium value and decrease the critical velocity for cavity formation. When a soap bubble layer is present, subsurface cavities form at all impact velocities. Our analysis shows that the bubble layer wets the sphere prior to impact with a patchy coating of droplets and bubbles. The droplets alter the splash and create an aperture for air entrainment, which leads to cavity formation at wetted locations on the sphere surface. The water-surfactant entry behavior of these partially wetted spheres results in a progression of cavity formation regimes with increasing Weber number, similar to the cavity regimes of hydrophobic spheres entering water. Nonuniform droplet coatings create cavity asymmetries altering transitions between these regimes.

DOI: 10.1103/PhysRevFluids.3.104004

I. INTRODUCTION

When a rigid sphere impacts a liquid surface with sufficient velocity it creates a splash crown and an air-filled subsurface cavity [1]. At low impact velocities, the splash crown adheres to the sphere, climbs up its surface, and meets itself at the apex, suppressing cavity formation. Duez *et al.* [2] showed that the behavior of the splash and consequently the presence or absence of a subsurface cavity for a smooth sphere depends on liquid surface tension (σ), viscosity (μ), static wetting angle (θ), and sphere impact velocity (U). For hydrophilic or wetting spheres ($\theta < 90^\circ$) cavities form when the impact occurs above a constant critical velocity, U_{cr}. For hydrophobic or nonwetting spheres ($\theta > 90^\circ$), the value of U_{cr} decreases with increasing θ [2]. Zhao *et al.* expanded this work by showing that cavity formation also depends on sphere roughness R_z with the critical velocity for cavity formation decreasing with increasing roughness [3].

Aristoff and Bush investigated cavities formed by small nonwetting spheres, identifying four distinct cavity types named quasistatic, shallow, deep, and surface seal cavities [4]. Spheres that are half wetting and half nonwetting produce asymmetric cavities and curved trajectories beneath

*taddtruscott@gmail.com

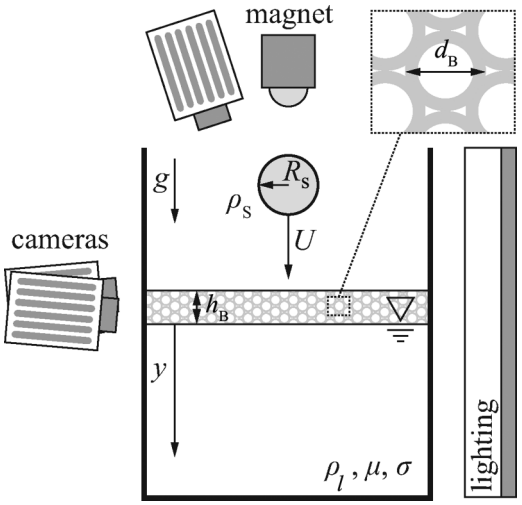

FIG. 1. (a) Stainless steel spheres of radius R_s and density ρ_s were dropped from an electromagnet into a glass tank, impacting the liquid surface with velocity U. The tank was filled with a water-surfactant mixture having density ρ_l, viscosity μ, and surface tension σ. For some experiments the water-surfactant mixture was covered with a bubble layer of height h_B composed of average bubble diameters d_B.

the free surface as shown by Truscott and Techet [5] and Bodily *et al.* [6] for slender torpedo-like bodies. Although the wettability of an object is important to water entry behavior, one might wonder what will happen if an object is partially wetted before entry. Cavity formation characteristics in surfactant mixtures, pools covered with a bubble layer, or partially prewetted projectiles have not been addressed previously.

Herein, we first examine the effect of a surfactant on the critical velocity necessary for a sphere to form a cavity during free-surface entry. Second, bubbles commonly form in surfactant mixtures, and observations show that spheres that pass through a bubble layer before free-surface entry create cavities at lower impact velocities than anticipated. Hence, we examine the principle mechanism by which bubbles cause these unanticipated cavities (i.e., partial wetting). We then report on the cavity formation types.

II. EXPERIMENTAL SETUP

A schematic of the experimental setup is represented in Fig. 1. Experiments were performed with smooth ($R_z = 0.6 \pm 0.3\ \mu$m) stainless steel spheres ($\rho_S = 7750$ kg/m^3) with radii $R_s = 1.59$–12.70 ± 0.0025 mm. Spheres were dropped into a glass tank ($40 \times 40 \times 122$ cm^3) from an electromagnet. Drop height was varied to alter impact velocity U at the water-free surface from approximately 0.44 to 7.67 m/s, representing a parameter space where sphere deceleration is negligible during cavity formation and collapse [7]. The impact event was filmed using three Photron SA3 high-speed cameras with diffuse backlighting. Two cameras were used to film both above and below the free surface from the side, and a third camera captured the entry event from above for a top-down view. Close-up color images were taken with a Phantom v2511. Critical dimensionless numbers and and their ranges for this study include Froude number ($\mathrm{Fr} = U^2/gR_s$: 1.6–3800), Weber number ($\mathrm{We} = \rho_l U^2 R_s/\sigma_e$: 11–23 000), and Bond number ($\mathrm{Bo} = \rho_l g {R_s}^2/\sigma_e$: 0.91–58), where σ_e is the equilibrium surface tension of the water-surfactant mixture.

The glass tank was filled with a water-surfactant mixture made with Ajax dish soap (189 parts water to 1 part soap, by volume). Ajax dish soap is composed of several different chemicals, four of which act as surfactants to decrease the surface tension: ammonium lauryl sulfate, ammonium laureth sulfate, lauramidopropylamine oxide, and poloxamer 124. The water-surfactant mixture was

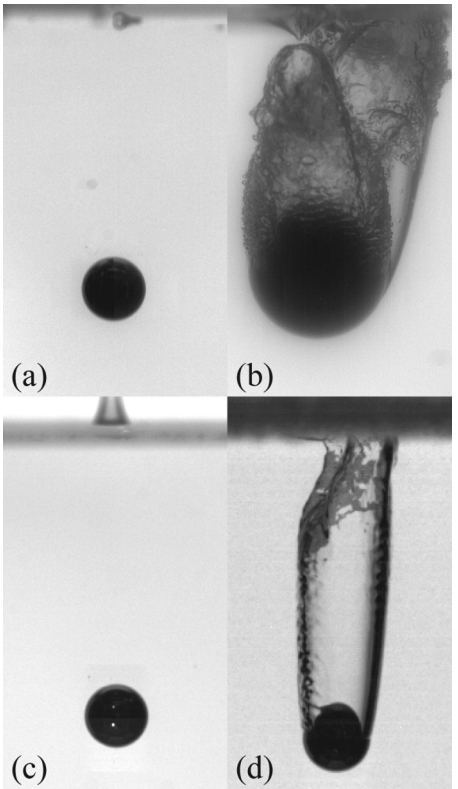

FIG. 2. Images show the impact of smooth, wetting stainless steel spheres onto the water-surfactant mixture. (a) A sphere of radius $R_s = 4.76$ mm impacts the mixture at $U = 5.42$ m/s without forming a cavity. (b) A larger sphere ($R_s = 11.11$ mm) impacts the pool at the same velocity forming a messy cavity. (c) A sphere of radius $R_s = 4.76$ mm impacts the pool at $U = 2.43$ m/s without forming a cavity. (d) A sphere with the same impact conditions as in (c) passes through a bubble layer prior to the free surface impact and creates an asymmetric subsurface cavity. See supplemental videos 1–4 that correspond to panels (a)–(d), respectively [21].

characterized by the following physical properties: density $\rho_l = 999$ kg/m^3, viscosity $\mu = 1.09 \pm 0.01 \times 10^{-3}$ Pa s, equilibrium surface tension $\sigma_e = 27.3 \pm 0.2$ mN/m, and stainless steel advancing static contact angle $\theta = 30^\circ \pm 4^\circ$. Experimental work with the surfactant mixture was not performed for more than three days. Liquid properties (μ, σ_e, and θ) were measured with each new water-surfactant mixture, with 95% confidence of the mean values listed above. Surface bubble layers were created for heights h_B ranging 5–100 mm, which comprised bubble diameters d_B in the range of 1–20 mm.

III. RESULTS

Figure 2 displays images of smooth, wetting spheres impacting the water-surfactant mixture at various impact conditions. In Fig. 2(a) a sphere with radius $R_s = 4.76$ mm impacts the pool with a velocity of $U = 5.42$ m/s without forming a cavity. This impact velocity is much higher than the critical velocity for cavity formation for the equilibrium water-surfactant mixture as predicted by Duez *et al.* [2] ($U_{\rm cr} = 0.1\sigma_e/\mu \approx 2.5$ m/s). In Fig. 2(b) a larger sphere ($R_s = 11.11$ mm) impacts at the same velocity forming a cavity. Hence, we see that the critical velocity for cavity formation is dependent on R_s in a water-surfactant mixture. In Fig. 2(c) a sphere with radius $R_s = 4.76$ mm impacts the pool at $U = 2.43$ m/s without forming a cavity, but in Fig. 2(d) a sphere with the same

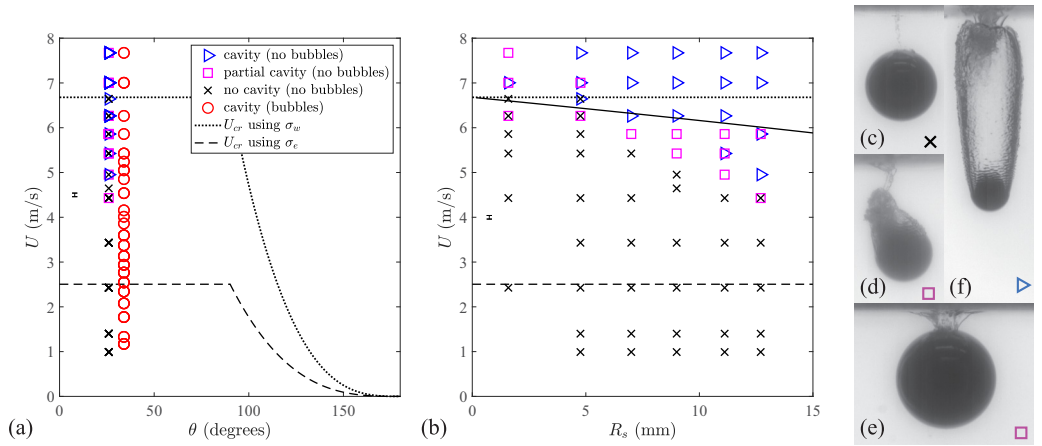

FIG. 3. (a) The critical velocity for cavity formation by spheres impacting onto a water-surfactant mixture for both a clean pool surface (no bubbles) and with a bubble layer resting on the surface is shown. Cavities form at all impact velocities when spheres first pass through a bubble layer. All the spheres are made of the same steel with static contact angle $\theta = 30^\circ \pm 4^\circ$, but the data are spread between $26^\circ < \theta < 34^\circ$ for readability. (b) The critical velocity for cavity formation on a clean pool surface decreases as the sphere radius increases. At low impact velocities on a clean surface, spheres do not form cavities as shown in (c) although small bubbles may be pulled under the surface. A transitional region is seen in which small asymmetric air pockets (d) and small cavities (e) form, which we call partial cavities. At the highest velocities full cavities form (f). Theoretical estimates for $U_{\rm cr}$ for water ($\cdots$) and the water-surfactant mixture ($--$) are based on Duez *et al.* [2]. The solid-black line represents (3) and appears only in (b). The uncertainty bands show the 95% confidence interval on the mean impact velocities.

radius and velocity forms a cavity after first passing through a bubble layer resting on the pool surface.

We first examine the effect of surfactant on the critical velocity for cavity formation $U_{\rm cr}$ for a clean free surface (no bubbles). As shown in Fig. 3(a), cavity formation in the water-surfactant mixture does not occur at a constant $U_{\rm cr}$. Rather, as shown in Fig. 3(b), $U_{\rm cr}$ varies with R_s, where $U_{\rm cr}$ is approximately equal to the critical velocity in pure water for small R_s and decreases towards the predicted critical velocity [2] of the equilibrium surfactant mixture as R_s increases. Hence, $U_{\rm cr}$ for a water surface mixture lies between the Duez prediction for water and a water-surfactant mixture.

To explain the dependence of $U_{\rm cr}$ on R_s we examine the influence of dynamic surface tension $\sigma_d(t)$. Upon sphere impact a splash crown forms, which locally increases the surface area of the pool. When the surface expands the surface density of the surfactant decreases, which increases the local surface tension above the equilibrium value σ_e [8]. At this point, the surface tension of the newly formed surface begins to decrease back towards σ_e as surfactant molecules adsorb to the newly formed surface [9]. The time required for the dynamic surface tension $\sigma_d(t)$ to decrease from the value of water σ_w to σ_e will be denoted as t_o and is estimated using the pendant bubble technique [10] described in the Appendix. Using this technique we found t_o to decrease as the initial expansion velocity of the bubble (local advection) increases, similar to the findings of He *et al.* [11], Moorkanikkara and Blankschtein [12], and Alvarez *et al.* [13]. The full surface tension drop time for the given water-surfactant mixture can be approximated by $t_o = (\sigma_w - \sigma_e)/m$, where m is the rate at which the surface tension decreases, and is described by the fit $m = aU^b$, where $a = 1.42$, $b = 0.49$ (see the Appendix for more details). Using these equations we estimate t_o using the two critical velocities shown in Fig. 3(a) (2.5 and 6.7 m/s) and find $t_o \approx 13$–20 ms.

We now compare t_o to the duration of the splash formation, calculated here as half the submergence time R_s/U, to estimate the dynamic surface tension in the splash and approximate $U_{\rm cr}$ for the water-surfactant mixture. Using the transition data in Fig. 3(b) we see that $R_s/U < 3$ ms.

Hence, $R_s/U < t_o$ and $\sigma_d(t)$ does not have sufficient time to reach equilibrium, but rather decreases to a value between σ_w and σ_e. Therefore, at a certain impact velocity, U, a larger sphere takes longer to submerge than a small one, and thus has more time for surfactant molecules to adsorb to the newly formed surface decreasing the surface tension and consequently U_{cr} as shown in Fig. 3(b). Quantitatively, if we assume the drop in the surface tension from σ_w to σ_e is linear with time (see the Appendix) we can write the following equation to estimate the dynamic surface tension at the time the sphere is half submerged, $\sigma_d(R_s/U)$:

$$\frac{\sigma_w - \sigma_d(R_s/U)}{R_s/U} = m. \tag{1}$$

Solving for $\sigma_d(R_s/U)$ we substitute this into the equation found by Duez *et al.* [2] for the critical velocity ($U_{\mathrm{cr}} = 0.1\sigma/\mu$) and obtain

$$U_{\mathrm{cr}} = \frac{0.1}{\mu}\left(\sigma_w - \frac{mR_s}{U}\right). \tag{2}$$

Using the fit for m and noting that transition occurs when $U_{\mathrm{cr}} = U$, we rearrange to find an approximation for U_{cr} in the water-surfactant mixture described by

$$R_s = \frac{1}{a}U_{\mathrm{cr}}^{1-b}(\sigma_w - 10\mu U_{\mathrm{cr}}). \tag{3}$$

Equation (3) is plotted in Fig. 3(b), and although it does not divide the cavity and no cavity regions very well, it does show the dependence of U_{cr} on R_s and divides the partial cavity and full cavity regimes. In order to improve the prediction of U_{cr} a better method of measuring the dynamic surface tension for large impact velocities (high advection rates) and similar geometry [14,15] is required.

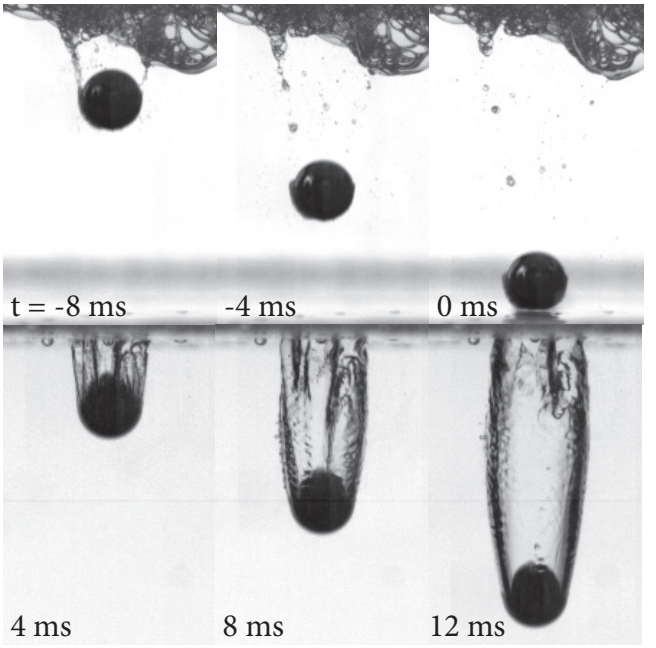

FIG. 4. This sequence of images shows a sphere ($R_s = 4.76$ mm) exiting a bubble-filled tube ($t = -8$ to 0 ms) and impacting the pool surface ($t = 4$ to 12 ms). Several bubble films are ruptured when the sphere passes through the bubbles, wetting the sphere surface with small droplets and bubbles. When this wetted sphere impacts the pool a cavity forms. See supplemental videos 5 and 6 [21].

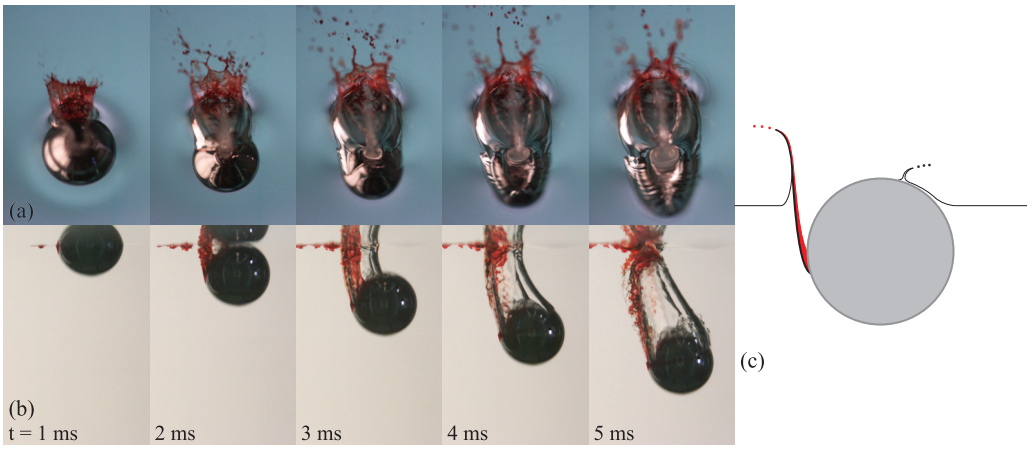

FIG. 5. Image sequences of two independent events recorded from (a) top and (b) side views where a stainless steel sphere ($R_s = 4.76$ mm) enters tap water with a droplet of red dye placed at its equator prior to release. The spheres impact water with identical velocities U, less than the critical velocity for air entrainment U_{cr}. The droplet deforms upon impact ($t = 1$ ms), spreading into the splash (a) and left edge of the cavity (b) to initiate cavity formation. The cavity and splash form only in the vicinity of the droplet with water climbing up the sphere surface in all other locations. The contact line moves towards the sphere apex ($t = 2-3$ ms), the cavity expands and moves down the other side towards the equator at $t = 4$–5 ms. Supplemental videos 7 and 8 correspond to (a) and (b), respectively [21]. (c) The schematic shows droplet deformation pushing water away from the sphere near the equator in a manner reminiscent of nonwetting coatings [1].

To our knowledge such a method has not yet been developed, and hence we leave an improved prediction of the critical velocity in a water-surfactant mixture for future research.

As the entry event transitions from non-cavity-forming [Fig. 3(c)] to cavity-forming cases [Fig. 3(f)], an intermediate stage is seen in which two types of partial cavities form, similar to the observations of Marston *et al.* [16] in the water entry of Leidenfrost spheres. The first occurs when cavity formation initiates only at small localized sections of the sphere leading to a rapid pinch-off and a small asymmetric air pocket as seen in Fig. 3(d). The second generally occurs for larger sphere radii when the splash moves up the sphere sides in a nonuniform manner leading to an asymmetric closure at the sphere apex and a passage for a small amount of air to be entrained under the surface [Fig. 3(e)].

When a bubble layer rests on the pool surface, cavities form at all impact velocities tested [Fig. 3(a)], regardless of varying h_B and d_B. To investigate why the presence of a bubble layer leads to cavity formation we dropped a sphere through a bubble-filled tube and examined it while exiting into the air as shown in Fig. 4. As the sphere passes through the bubble layer, ruptured soap films adhere to the sphere forming small droplets and bubbles. The bubble layer thus partially wets the sphere prior to the free surface impact resulting in cavity formation.

To examine the mechanism by which small droplets on the sphere surface initiate cavity formation we place a single droplet of miscible red dye (food coloring, $\mu = 2.50 \times 10^{-3}$Pa s, $\sigma = 55.5$ mN/m, and $\theta = 80^\circ \pm 2^\circ$) near the equator of a clean sphere before dropping it into tap water. Two separate impact events were recorded from top and side views [Figs. 5(a) and 5(b)] and aligned from the time of impact ($t = 0$). When the sphere is approximately half submerged ($t = 1$ ms), the dye droplet impacts the pool, causing it to deform into a thin sheet, extending upward into the splash and initiating cavity formation [Fig. 5(c)]. As the droplet deforms, it pushes water away from the sphere near the equator in a manner reminiscent of nonwetting coatings [1]. While water advances up the unwetted portion of the sphere, the detachment created by the dye droplet results in a splash and a means for air entrainment, leading to cavity formation in the droplet vicinity. This localized cavity formation results in an asymmetric cavity that resembles those created

by the water entry of half-wetting spheres [5] and produces lateral motion. As the sphere descends further into the liquid, the droplet of dye continues to coat the cavity wall and deflect water away from the sphere ($t = 2$–3 ms). The contact line, initially existing on only one sphere side, expands upward to unwet the sphere as it moves towards the apex and down the other side; the cavity expands and effectively shifts contact from the upper-left side of the sphere [Fig. 5(b)] to the trailing side ($t = 2$–5 ms). A similar sequence of events is observed when a sphere falls through a bubble-filled tube followed by an air gap before impacting a clean pool surface (as seen in Fig. 4).

The cavity formed by placing a droplet of dye on a clean sphere initially resembles that formed by a single droplet impact [17]. When a single droplet impacts a pool it spreads out on the surface, pushing the fluid both downward and outward with the droplet liquid spreading over the surface of the newly formed cavity. The initial impact of a liquid jet on a pool behaves in the same way [18,19]. The combination of the two impact types (solid-liquid and liquid-liquid) causes wetting spheres to form cavities similar to those formed by nonwetting or rough spheres.

A similarity between nonwetting spheres and wetting spheres that pass through a bubble layer prior to impact is noted in the cavity types observed in Fig. 6. For the lowest We values, pinch-off occurs on or very near the sphere surface which is described as quasistatic seal [Fig. 6(a)]. As the Weber number reaches We $\approx$ 800, 400, and 2300, for Bo $=$ 0.91, 8.2, and 58, respectively, a larger cavity forms a shallow seal [Fig. 6(b)]. When We $\approx$ 6000 for Bo $=$ 58, pinch-off occurs approximately midway between the sphere and free surface, resulting in a deep seal [Fig. 6(c)]. At the highest values, We $\gtrsim$ 1300, 2400, and 9000 for Bo $=$ 0.91, 8.2, and 58, respectively, the splash crown domes over leading to surface seal [Fig. 6(d)]. These cavity regimes were identified by Aristoff and Bush [4], who obtained the same progression of regimes with increasing We for small nonwetting spheres with a similar comparison for h_p and We as seen in Fig. 6(e). When looking specifically at the deep seal cases, h_p scales better with Fr as shown in the inset, with h_p slightly less than the predicted value[7] similar to the data of Aristoff *et al.* [7] for steel spheres in pure water.

Prewetting of wetting spheres in a water-surfactant mixture does not lead to a perfect overlap of pinch-off regimes found by Aristoff and Bush [4]. For instance, the shallow seal events observed occurring at Bo $=$ 58 [Fig. 6(e)] do not correspond with previously published results [4]. The discrepancy is brought about in part by nonuniform wetting as the sphere passes through the bubble layer, resulting in asymmetric cavities. This nonuniformity can in turn lead to an asymmetric cavity collapse as seen in Fig. 6(b) (evidenced by the wide pinch-off point). The asymmetries are most prominent near the pool surface, before the cavity has migrated to the sphere wake. This effect can lead to much narrower cavity diameters near the surface affecting the quasistatic, shallow, and surface seal regimes more significantly. The phenomenon is more pronounced for the two smaller sphere radii where asymmetries near the pool surface cause shallow seal to occur rather than deep seal. Although the cavity asymmetries are caused by the asymmetric adhesion of droplets on the sphere surface, no trends were observed in the cavity types with changes in the bubble layer height (h_B) or bubble diameter (d_B). The discrepancy in the pinch-off regime transitions could also be explained by the change in $\sigma_d(t)$ over time, with the surface tension in the splash and on the cavity walls approaching σ_w during the early moments after surface creation and subsequently decreasing toward σ_e as surfactant molecules adsorb. This would initially result in lower values of Bo and We that would increase over a short period.

IV. CONCLUSION

In conclusion, our experimental results show that the addition of a surfactant to a pool of water causes the surface tension to vary with time, thus altering the critical velocity for cavity formation and causing it to vary with sphere radius. The presence of a bubble layer resting on the surface of a water-surfactant mixture leads to the formation of subsurface cavities at all impact velocities tested. By observing a sphere falling through a bubble layer suspended above the free surface, we note that bursting bubbles lead to the formation of small droplets and bubbles on the sphere surface.

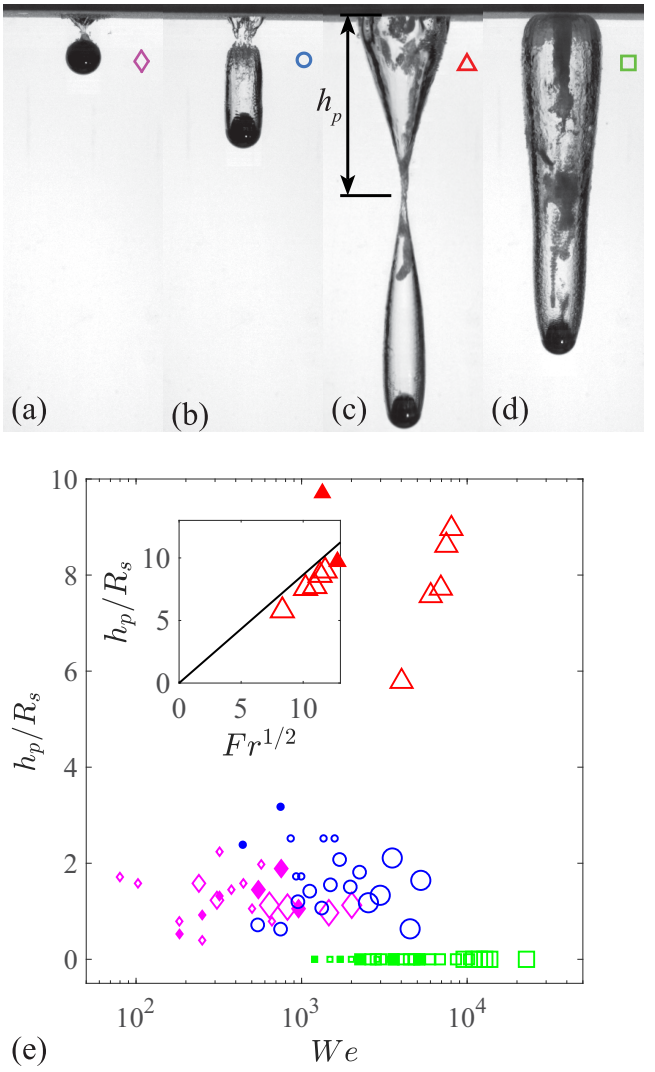

FIG. 6. Cavity regimes observed with increasing Weber numbers transitioning from (a) quasistatic seal to (b) shallow seal, to (c) deep seal, and (d) surface seal shown for Bo = 58 (R_s = 12.70 mm). All cavity types were formed by stainless steel spheres (θ = 30°) entering a pool of water-surfactant mixture through a bubble layer resting on the free surface. Supplemental videos 9–12 correspond to panels (a)–(d), respectively [21]. (e) The nondimensional pinch-off depth, h_p/R_s, is plotted as a function of We with symbol size increasing for increasing Bo (Bo = 0.91, 8.2, and 58). Hollow symbols represent impact cases with bubbles on the pool surface, and solid symbols represent cases where spheres passed through a bubble tube elevated above the pool surface. The inset shows that for deep seal h_p scales better with Fr with the solid line showing the prediction of Aristoff *et al.* [7]. The pinch-off depth h_p is defined in (c).

Rather than enhancing the wettability of a sphere, these droplets disrupt the advancing fluid and alter the splash, which leads to air entrainment and cavity formation under conditions where this would not normally be expected. The prewetted spheres mimic the water-entry behavior of nonwetting spheres; forming the same four cavity regimes (i.e., quasistatic, shallow, deep, and surface seal). But the nonuniform droplet coatings cause cavity asymmetries that disrupt transitions between these

regimes. It is also possible that the surfactant may disrupt the pinch-off transitions due to dynamic surface tension effects, which could be investigated further in future studies.

ACKNOWLEDGMENTS

N.S., R.H., and T.T.T. acknowledge funding by the Office of Naval Research, Navy Undersea Research Program (Grant No. N0001414WX00811). We thank Randy Ewoldt and Jan Vermant for helpful discussions and insight into dynamic surface tension.

APPENDIX: PENDANT BUBBLE METHOD

Previous research on dynamic surface tension generally focuses on low Péclet number experiments where diffusion is the dominant transport mechanism of the surfactant molecules to the interface and advection is minimal [14,20]. However, in our experiments the Péclet number $\mathrm{Pe} = O(10^4)$, indicating that advective mass transport dominates over diffusive mass transport. Moorkanikkara and Blankschtein showed that the commonly used pendant bubble technique for measuring dynamic surface tension inherently induces convective currents that increase the rate of surfactant transport and hence adsorption to the interface [12]. Alvarez *et al.* induced a flow in their newly developed microtensiometer [15] to investigate the effects of advection and found that the surface tension decreases faster with increasing Pe. We exploit the inherent flow in the pendant bubble technique to find an estimate of the rate at which our surfactant decreases the surface tension of newly formed interface.

To find the time t_o for the surfactant to decrease the surface tension from water σ_w to the equilibrium value of the surfactant σ_e, we use the pendant bubble technique, which has similar geometry to a sphere entering water [14]. To do this we blow a bubble out of a nozzle into the water-surfactant mixture and video record the growth and shape of the bubble at 3000 frames per second, as shown in Fig. 7(a). We expand the bubble quickly at first to induce a flow over its surface and then more slowly so that we can observe the shape change with time. We then track the radii of curvature at the tip and right-hand side of the bubble as shown in Fig. 7(b) and use the Young-Laplace equation to calculate the pressure drop across the interface. Using the height between these two positions on the bubble we can calculate the surface tension for each frame.

The surface tension is calculated as follows. Applying the Young-Laplace equation on the right-hand side of the bubble we obtain

$$P_b - P_1 = \sigma_d \left(\frac{1}{R_1} + \frac{1}{R_2} \right). \tag{A1}$$

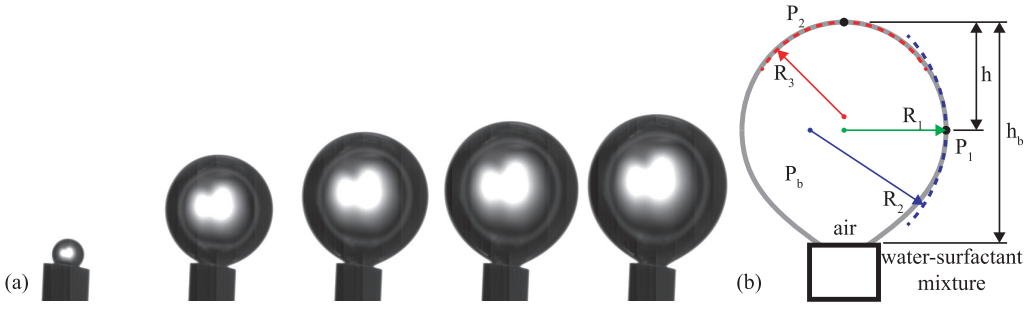

FIG. 7. (a) An air bubble is blown out of a nozzle (0.5 mm OD), expanding very quickly at first and then more slowly over time. The time between images is 10 ms. (b) The various radii and lengths measured from each image are labeled.

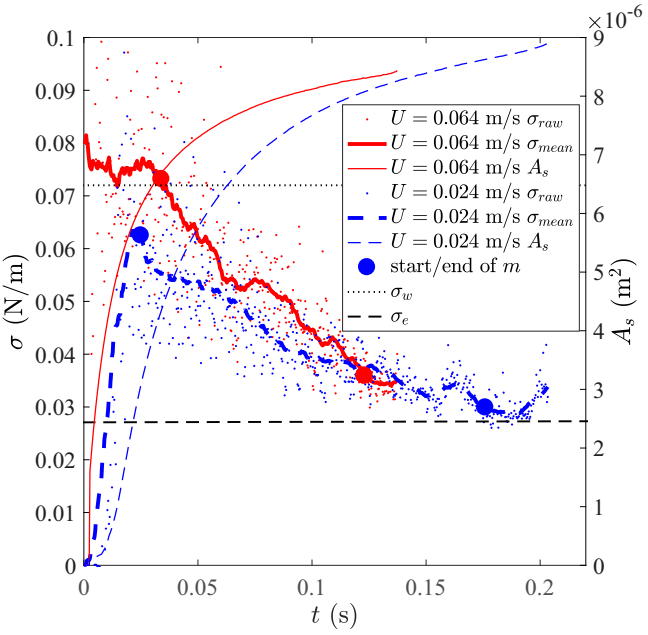

FIG. 8. Two example measurements of the surface tension over time using the pendant bubble method are shown. The small dots show the raw surface tension data calculated from (A3), and the thick solid and dashed lines show the moving mean over a window of 17 ms. The surface tension drop rate m is calculated by taking the slope between the large blue and red dots. The thin solid and dashed lines show the approximate surface area A_s of the bubble over time.

The top has only one radius of curvature due to the axisymmetry of the bubble, so the Young-Laplace equation is

$$P_b - P_2 = 2\frac{\sigma_d}{R_3}. \tag{A2}$$

Noting that $P_1 = P_2 + \rho g h$, subtracting (A1) from (A2) and rearranging we obtain

$$\sigma_d = \frac{\rho g h}{\frac{2}{R_3} - \frac{1}{R_1} - \frac{1}{R_2}} \tag{A3}$$

for a specific instance in time.

Figure 8 shows two cases of the change in σ_d over time with the corresponding change in the surface area of the bubble. From these plots we estimate the rate at which the surface tension decreases by finding the slope m of a line drawn between the large blue and red dots shown in Fig. 8 for each case. The starting position (first large dot) is chosen as the location where σ_d drops below σ_w or as the peak if that is not available. The ending position (second large dot) is chosen as the point where σ_d begins to flatten out near σ_e.

The surface tension decreases faster as the initial expansion velocity of the bubble U increases (Fig. 9, the initial expansion velocity is defined in the inset). Due to limitations of the setup, only expansion velocities in the range of $U = 0.017$–0.361 m/s could be achieved. Hence, for extrapolations purposes we fit the pendant bubble data in Fig. 9 to the equation $m = aU^b$ and find $a = 1.42$ and $b = 0.49$. (Note that a must have units of kg s^{b-3}m^{-b} if U has units of ms^{-1} and m has units of Nm^{-1} s^{-1}.) The time required for the surface tension to drop from σ_w to σ_e can then be calculated as $t_o = (\sigma_w - \sigma_e)/m$. Extrapolating the fit out to the range of the spheres' impact velocities, we can estimate t_o for the sphere impacts.

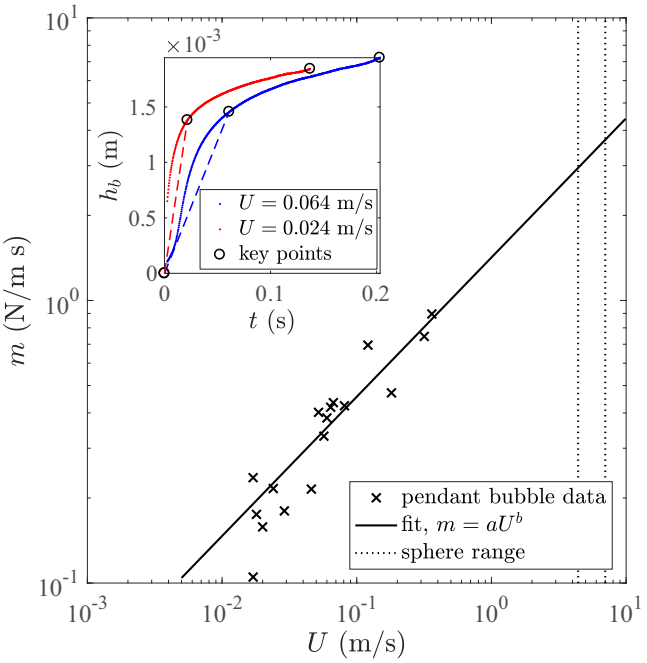

FIG. 9. The surface tension drop rate m is shown to depend on the liquid flow rate over the bubble U. The solid line is the fit to the pendant bubble data, $m = aU^b$, where $a = 1.42$ and $b = 0.49$, which we extrapolate out to the sphere impact velocities $(\cdots)$. The inset shows the method for calculating U for the same two cases in Fig. 8. The position of the bubble tip h_b is tracked over time, and the velocity U is taken as the slope of the line from $h_b = 0$ to 75% of the maximum h_b (all indicated with open circles).

[1] T. T. Truscott, B. P. Epps, and J. Belden, Water entry of projectiles, Annu. Rev. Fluid Mech. **46**, 355 (2014).

[2] C. Duez, C. Ybert, C. Clanet, and L. Bocquet, Making a splash with water repellency, Nat. Phys. **3**, 180 (2007).

[3] M.-H. Zhao, X.-P. Chen, and Q. Wang, Wetting failure of hydrophilic surfaces promoted by surface roughness, Sci. Rep. **4**, 5376 (2014).

[4] J. M. Aristoff and J. W. M. Bush, Water entry of small hydrophobic spheres, J. Fluid Mech. **619**, 45 (2009).

[5] T. T. Truscott and A. H. Techet, A spin on cavity formation during water entry of hydrophobic and hydrophilic spheres, Phys. Fluids **21**, 121703 (2009).

[6] K. G. Bodily, S. J. Carlson, and T. T. Truscott, The water entry of slender axisymmetric bodies, Phys. Fluids **26**, 072108 (2014).

[7] J. M. Aristoff, T. T. Truscott, A. H. Techet, and J. W. M. Bush, The water entry of decelerating spheres, Phys. Fluids **22**, 032102 (2010).

[8] Y.-C. Liao, O. A. Basaran, and E. I. Franses, Effects of dynamic surface tension and fluid flow on the oscillations of a supported bubble, Colloids Surf. A **282–283**, 183 (2006).

[9] A. F. H. Ward and L. Tordai, Time-dependence of boundary tensions of solutions I. The role of diffusion in time-effects, J. Chem. Phys. **14**, 453 (1946).

[10] E. I. Franses, O. A. Basaran, and C.-H. Chang, Techniques to measure dynamic surface tension, Curr. Opin. Colloid Interface Sci. **1**, 296 (1996).

[11] Y. He, P. Yazhgur, A. Salonen, and D. Langevin, Adsorption–desorption kinetics of surfactants at liquid surfaces, Adv. Colloid Interface Sci. **222**, 377 (2015).

[12] S. N. Moorkanikkara and D. Blankschtein, Possible existence of convective currents in surfactant bulk solution in experimental pendant-bubble dynamic surface tension measurements, Langmuir **25**, 1434 (2009).
[13] N. J. Alvarez, D. R. Vogus, L. M. Walker, and S. L. Anna, Using bulk convection in a microtensiometer to approach kinetic-limited surfactant dynamics at fluid–fluid interfaces, J. Colloid Interface Sci. **372**, 183 (2012).
[14] N. J. Alvarez, L. M. Walker, and S. L. Anna, Diffusion-limited adsorption to a spherical geometry: The impact of curvature and competitive time scales, Phys. Rev. E **82**, 011604 (2010).
[15] N. J. Alvarez, L. M. Walker, and S. L. Anna, A microtensiometer to probe the effect of radius of curvature on surfactant transport to a spherical interface, Langmuir **26**, 13310 (2010).
[16] J. O. Marston, I. U. Vakarelski, and S. T. Thoroddsen, Cavity formation by the impact of Leidenfrost spheres, J. Fluid Mech. **699**, 465 (2012).
[17] O. G. Engel, Crater depth in fluid impacts, J. Appl. Phys. **37**, 1798 (1966).
[18] B. Kersten, C. D. Ohl, and A. Prosperetti, Transient impact of a liquid column on a miscible liquid surface, Phys. Fluids **15**, 821 (2003).
[19] Y. Zhu, H. N. Oğuz, and A. Prosperetti, On the mechanism of air entrainment by liquid jets at a free surface, J. Fluid Mech. **404**, 151 (2000).
[20] J. Eastoe and J. S. Dalton, Dynamic surface tension and adsorption mechanisms of surfactants at the air–water interface, Adv. Colloid Interface Sci. **85**, 103 (2000).
[21] See Supplemental Material at http://link.aps.org/supplemental/10.1103/PhysRevFluids.3.104004 for corresponding videos.